Biochemical and Biophysical Research Communications 490 (2017) 1093–1099

Contents lists available at ScienceDirect

Biochemical and Biophysical Research Communications

journal homepage: www.elsevier.com/locate/ybbrc

# A novel conformation of the LC3-interacting region motif revealed by the structure of a complex between LC3B and RavZ

Do Hoon Kwon, Leehyeon Kim, Byeong-Won Kim, Jun Hoe Kim, Kyung-Hye Roh, Eui-Ju Choi, Hyun Kyu Song*

*Department of Life Sciences, Korea University, 145 Anam-ro, Seongbuk-gu, Seoul 02841, Republic of Korea*

ARTICLE INFO

*Article history:*
Received 21 June 2017
Accepted 28 June 2017
Available online 29 June 2017

*Keywords:*
Crystal structure
LC3
LIR motif
*Legionella pneumophila*
RavZ
Xenophagy

ABSTRACT

LC3-family member proteins play a critical role in autophagy, a cellular process responsible for the degradation of massive cellular components including intracellular pathogens. A variety of molecules involved in the autophagic pathway engage in specific interactions with a unique sequence motif referred to as the LIR (LC3-interacting region) motif. Although identification of conserved structural features of LIR motifs in complex with LC3-family members has established a canonical LIR motif, atypical conformations of LIR motifs have recently been revealed. Here, we determined the three-dimensional crystal structures of LC3B in complex with three different LIR motifs of RavZ from *Legionella pneumophila*, an intracellular pathogen that can manipulate the host autophagy system. The tandem LIR motifs located in the N-terminal region of RavZ adopt a novel β-sheet conformation and thus provide specific ionic interactions with LC3B in addition to canonical hydrophobic plugged-in interactions. Consequently, these motifs possess higher binding affinity to LC3-family members than canonical LIR motifs, although the tandem repeats can only bind to one LC3 molecule. These findings broaden our understanding of the functional repertoire of LIR motifs in autophagy.

© 2017 Elsevier Inc. All rights reserved.

## 1. Introduction

Macroautophagy (hereafter referred to as autophagy) is a conserved degradation pathway utilized for the removal of unnecessary or damaged intracellular components and organelles in eukaryotic cells [1,2]. Autophagy was initially thought to be a non-specific process, however a wide variety of recent studies investigating selective autophagy have emerged [3–6]. In contrast to non-selective autophagy, selective autophagy regulates the abundance of specific cargo molecules *via* autophagy receptors that target protein complexes, aggregates, invading microbes, and whole organelles into lysosomes [6–8]. These specific autophagy receptors link the autophagosome with target molecules, and thus interact with both target cargo and Atg8-family member proteins embedded on the autophagosomal membrane. It is known that ubiquitylation plays a critical role in marking specific target molecules, and ubiquitylated cargo are recognized by the ubiquitin binding domain of autophagy receptors [5]. All of these receptors have an LC3-interacting region (LIR) motif to facilitate targeting to the autophagosomal membrane.

Of the various cargo targeted by autophagy, intracellular bacterial pathogens represent one type of substrate that autophagy targets for degradation [9–12]. When infected by bacteria, host cells utilize the autophagy system to clear the invading pathogens. The process related to autophagic clearance of intracellular pathogens is referred to as “xenophagy”. To survive xenophagy, various pathogens have evolved strategies to block or overcome host-mediated autophagy. In particular, *Legionella pneumophila* utilizes the effector protein RavZ to inhibit xenophagy [13]. The RavZ protein secreted by *Legionella pneumophila* can localize onto the LC3-conjugated phagophore membrane and cleaves the C-terminus of phosphatidylethanolamine (PE)-conjugated Atg8-family member proteins such as LC3 and GABARAP. Similar to other ubiquitin-like (Ubl) proteins, Atg8-family member proteins possess a β-grasp domain and a short flexible C-terminal tail that typically ends with at least one glycine residue [14–17]. Furthermore, they are

* Corresponding author.
*E-mail address:* hksong@korea.ac.kr (H.K. Song).

http://dx.doi.org/10.1016/j.bbrc.2017.06.173
0006-291X/© 2017 Elsevier Inc. All rights reserved.

distinguished by the presence of one or two α-helices near their N-terminus, which are crucial for providing the interaction site for the LIR motif [18,19]. RavZ cleaves the peptide bond between a hydrophobic residue and the terminal glycine of PE-conjugated LC3. As a result, *Legionella pneumophila* can effectively inhibit xenophagy by removing LC3 from the autophagosomal or phagophore membrane [13,20–24].

LC3 recognizes the LIR motif containing the Ω-x-x-Ψ sequence, where Ω and Ψ represent aromatic and hydrophobic residues, respectively, and the two inner residues (-x-x-) can be any amino acid residue [25,26]. In general, the presence of one or more acidic residues are necessary immediately before the LIR motif. In our previous report [22], distinct LIR motifs at the N- and C-terminal tails of RavZ were identified. Using these LIR motifs, RavZ is able to bind two LC3 molecules separately. Intriguingly, the N-terminal tail of RavZ contains mysterious tandem LIR repeats (LIR1 and LIR2), while the C-terminal tail of RavZ possesses a canonical LIR sequence (LIR3). More recently, there is a report that the structure of RavZ-LC3 shows non-functional complex as authors described and that of LIR2-LC3 fusion protein displays a canonical binding mode [23,24]. However, the characteristics of the N-terminal tandem repeats of the LIR motif remain unclear. This paper provides the first description of structural details and a novel conformation adopted by the tandem repeat LIR motif. In contrast to the canonical LIR motif, the N-terminal tandem LIR repeats of RavZ are maintained by a specific β-sheet conformation. Furthermore, we determined that the unique conformation of the LIR motif can bind to LC3B more tightly than the canonical motif, suggesting that RavZ overwhelms the interaction between LC3B and intracellular proteins containing LIR motifs. These results shed light on our understanding of the manner by which bacterial effector proteins overcome host autophagy mechanisms at the molecular level.

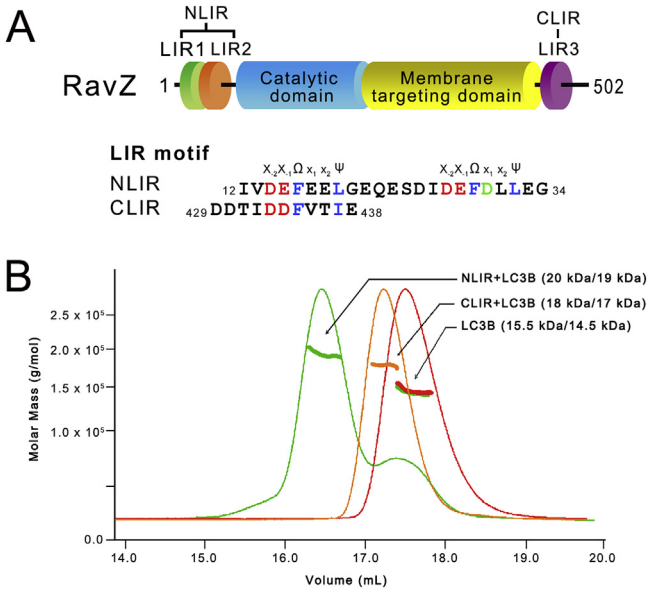


**Fig. 1.** Interaction between RavZ LIR peptides and LC3B. (A) Domain architecture of RavZ indicating the location of three LIR motifs (LIR1, LIR2 and LIR3). The abbreviations of each peptide used in this study are shown. Sequence of LIR motifs are aligned and the consensus motif $X_{-2}$-$X_{-1}$-Ω-$x_1$-$x_2$-Ψ (Ω: aromatic ring; Ψ: hydrophobic; $x_n$ and $X_n$ (n = 1, 2): any amino acid) is indicated. The critical hydrophobic phenylalanine and leucine (or isoleucine) residues in the F-$x_1$-$x_2$-L(I) motif are colored blue and the preceding 2 acidic residues ($X_{-2}$ and $X_{-1}$) are colored red. (B) The LC3B with NLIR (green line), LC3B with CLIR (orange line), and LC3B alone (red line) were analyzed by SEC-MALS. The horizontal line represents the measured molecular mass (MM). Excess LC3B with MM of 15 kDa elutes later. Each species is indicated by an arrow with experimental (MALS) and theoretically calculated (Calc) MM values shown in parentheses (MALS/Calc). This shows the 1:1 binding stoichiometry between RavZ peptides (NLIR and CLIR) and LC3B. Sequence information of each peptide is given in panel (A). (For interpretation of the references to colour in this figure legend, the reader is referred to the web version of this article.)

## 2. Materials and methods

The details of materials and methods are in the supplementary material.

## 3. Results

### *3.1. Each N-term and C-term LIR peptide binds to LC3B with 1:1 stoichiometry*

RavZ possesses three LIR motifs at flexible regions (Fig. 1A), and the N- and C-terminal tails of RavZ interact with LC3B separately as shown in our previous report [22]. However, it is unclear why tandem LIR motifs at the N-terminal region interact with only one LC3B. To clarify the role of this tandem repeat of LIR motifs, we performed SEC-MALS using RavZ LIR peptides (NLIR: residues 12–34 and CLIR: residues 429–438) and LC3B (Fig. 1B). Although two successive LIR motifs are present in the NLIR peptide of RavZ, the binding stoichiometry of NLIR and LC3B was determined to be 1:1, the same as for CLIR and LC3B. It indicated that two LC3B molecules are unable to bind simultaneously to the NLIR peptide. In an effort to characterize the feature of this NLIR of RavZ, structural studies of LC3B in complex with LIR peptides were initiated.

### *3.2. Structure of LC3B in complex with N-terminal tandem LIR motifs of RavZ*

As the LIR motifs of RavZ possess intrinsic flexibility and low binding affinity to LC3B, we failed to determine the structure of the RavZ-LC3B or LIR peptide-LC3B complexes. Instead, we generated the chimeric protein NLIR-LC3B ($RavZ^{12-34}$ + $MAP1LC3B^{2-120}$), which has been widely used for crystallization of the LC3B-LIR complex [27–29]. The structure of NLIR-LC3B was determined at 1.88 Å resolution. The overall structure of LC3B in the complex is virtually the same as previously reported LC3 structures, however, the structure of bound LIR differs from previously reported LIR structures (Fig. 2A). Each β-strand formed by residues belonging to the first LIR (LIR1) and second LIR (LIR2) motifs makes an anti-parallel β-sheet connected by a loop mimicking the shape of a horseshoe (Fig. 2A). LIR1 is bound to the pocket of LC3B whereas the second LIR motif (LIR2) does not bind to the pocket of LC3B. The LIR1 motif possesses the sequence $X_{-2}$-$X_{-1}$-Ω-$x_1$-$x_2$-Ψ (Fig. 1A), where Phe16 is located at the Ω (aromatic ring) position and Leu19 at the Ψ (hydrophobic) position. In general, the two residues ($x_1$ and $x_2$) between the characteristic aromatic and hydrophobic residues can be any amino acid residue since these do not participate in LC3B binding, although Glu18 at position $x_2$ in RavZ participates in LC3B binding (Fig. 2B and C). Two acidic residues Asp14 and Glu15 at positions $X_{-2}$ and $X_{-1}$, respectively, provide additional ionic interactions with positively charge residues of LC3B, which is quite common in the LIR-LC3B interaction [25,30]. As noted, the unusual secondary structure of the LIR2 motif is not directly involved with the hydrophobic binding pocket of LC3B, however, it provides an

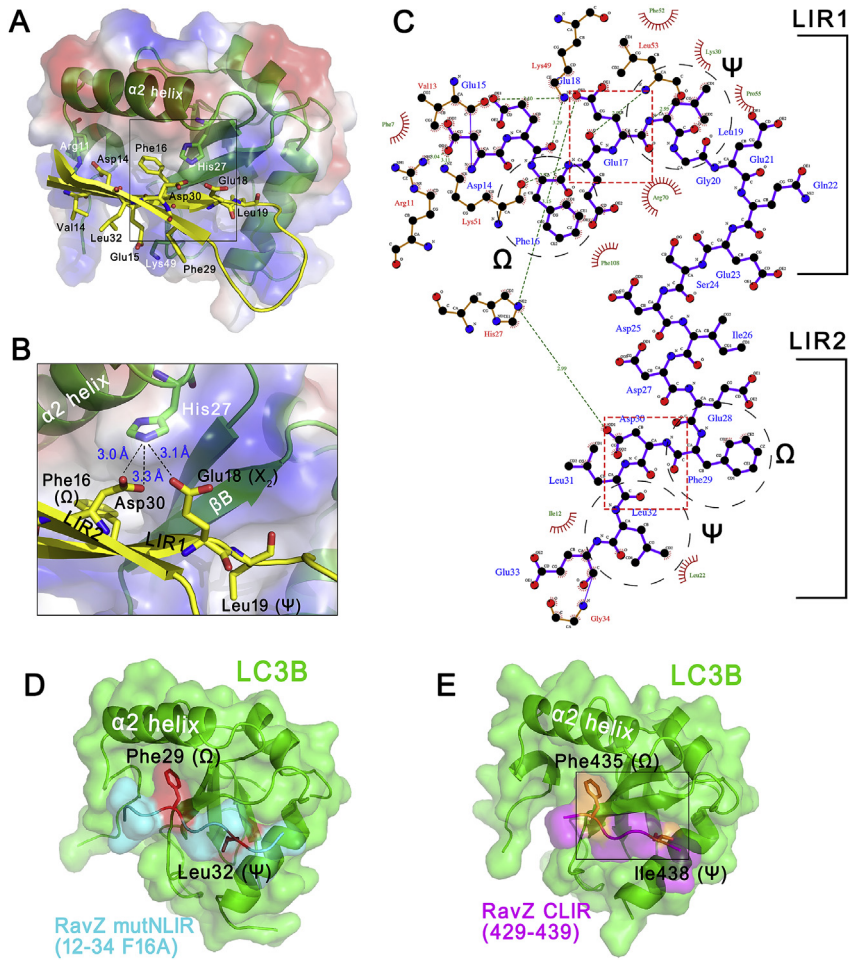


**Fig. 2.** Structures of LIR-LC3B complex. (A) Transparent electrostatic surface of LC3B in complex with NLIR peptide presented as a yellow ribbon diagram. The first β-strand possesses a canonical hydrophobic interaction *via* Phe16 (Ω) and Leu19 (Ψ) residues and several negatively charged residues are involved in the interaction between NLIR and LC3B. (B) Close-up view of additional polar interactions between NLIR and LC3B. Two negatively charged residues Glu18 and Asp30 from each LIR motif (LIR1 and LIR2) engage in ionic interactions with His27 of LC3B. The distances between the carboxylate oxygen atoms and imidazole ring nitrogen are indicated. Residues belonging to LC3B and NLIR are colored white and black, respectively. (C) Schematic of interactions between NLIR and LC3B. Hydrophobic interactions are indicated with red starbursts and hydrogen bonding interactions are shown as green dashed lines with hydrogen bonding distances. Residues belonging to NLIR and LC3B are labeled blue and red, respectively. The Ω and Ψ positions of LIR1 and LIR2 in NLIR are indicated with black dashed circles for clarity. Two acidic residues in NLIR engaged in additional polar interactions with His27 of LC3B are indicated with red dashed boxes. (D) Ribbon diagram with transparent surface of LC3B in complex with mutNLIR. The LIR2 motif is bound to LC3B *via* a canonical conformation. The region containing the LIR1 motif (residues 12–25) is invisible in the electron density map. (E) Ribbon diagram with transparent surface of LC3B in complex with CLIR. The bound CLIR to LC3B also shows a canonical conformation. (For interpretation of the references to colour in this figure legend, the reader is referred to the web version of this article.)

additional ionic interaction for higher binding affinity and specificity (see section 3.4 for details). This novel conformation of LIR motif was also shown in the structure of the construct with two more glycine residues inserted into the linker region of NLIR-LC3B ($RavZ^{12-34}$-Gly-Gly-LC3B; GG in Table 1) crystallized in different crystalline lattice.

### 3.3. Structures of LC3B in complex with LIR2 and LIR3 of RavZ

We attempted to obtain the structure of LC3B in complex with the LIR2 motif but found the task problematic. Therefore, a mutation of phenylalanine 16 to alanine was introduced to disrupt the interaction between LIR1 and LC3B. The chimeric protein with the F16A mutation of mutNLIR-LC3B was generated and crystallized with different crystal packing (Table 1). As expected, the mutant NLIR peptide was now bound to LC3B using the second LIR motif, LIR2 (Fig. 2D). In the mutNLIR-LC3B structure, the electron density of only 9 of the 23 residues was clearly visible (residues 26–34), while that of the LIR1 region was completely invisible. Furthermore, the conformation of LIR2 shows a canonical LIR binding mode found in many LC3B-bound structures including very recently reported RavZ LIR2-LC3 structure [23]. As described in the earlier section, the NLIR consists of two LIR motifs however, only one of these binds to LC3B (Fig. 1B). In an effort to examine why two LC3B molecules could not interact simultaneously with tandem LIR motifs, the structure of mutNLIR-LC3B was superposed onto the LIR2 region of NLIR-LC3B structure. The artificial 1:2 stoichiometric complex between NLIR and LC3B shows significant steric hindrance. This modeling clearly shows that two LC3B molecules are unable to interact simultaneously with two tandem repeat LIR motifs of N-terminal RavZ.

Since the structures of two LIR motifs at the N-terminal region in complex with LC3B have been determined, the structure of the chimeric protein CLIR-LC3B ($RavZ^{429-438}$ + $MAP1LC3B^{2-120}$) was also determined at 1.7 Å resolution (Fig. 2E). As expected, this binding mode is very similar to the canonical LIR binding mode

**Table 1**
Data collection and refinement statistics.

| | NLIR-LC3B | mutNLIR-LC3B | CLIR-LC3B | GG |
|---|---|---|---|---|
| **Data collection** | | | | |
| Beamline | PF-AR NE3A | PF-AR NE3A | PAL 5C | Home |
| Space group | $P4_32_12$ | $P1$ | $P2_1$ | $I4_122$ |
| Cell dimensions | | | | |
| *a*, *b*, *c* (Å) | 65.74, 65.74, 127.04 | 41.72, 53.44, 61.58 | 59.37, 73.64, 68.67 | 74.21, 74.21, 234.74 |
| α, β, γ (°) | 90, 90, 90 | 77.14, 73.17, 85.04 | 90, 101.37, 90 | 90, 90, 90 |
| Wavelength (Å) | 1.0000 | 1.0000 | 1.0000 | 1.54 |
| Resolution (Å) | 35.6–1.88 (1.95–1.88) | 32.1–2.00 (2.07–2.00) | 32.0–1.70 (1.76–1.70) | 37.1–3.30 (3.42–3.30) |
| $R_{merge}$ | 0.072 (0.533) | 0.070 (0.391) | 0.048 (0.575) | 0.094 (0.451) |
| $I/\sigma I$ | 50.56 (5.55) | 19.78 (2.10) | 37.86 (3.21) | 21.33 (5.36) |
| Completeness (%) | 99.5 (98.8) | 95.9 (86.2) | 99.7 (100.0) | 97.7 (99.2) |
| Redundancy | 8.8 (8.7) | 2.1 (1.9) | 4.1 (4.1) | 4.8 (4.9) |
| **Refinement** | | | | |
| Resolution (Å) | 1.88 | 2.00 | 1.70 | 3.30 |
| No. Reflections | 23,291 (2253) | 32,311 (2914) | 63,515 (6338) | 5173 (497) |
| $R_{work}/R_{free}$ | 21.1/26.0 | 21.2/26.2 | 21.4/25.0 | 28.0/34.2 |
| No. Atoms (total) | 2540 | 4369 | 4522 | 2183 |
| LC3B | 1957 | 3873 | 3821 | 1841 |
| RavZ | 390 | 284 | 216 | 335 |
| Water | 193 | 212 | 485 | 7 |
| *B*-factors (Å$^2$) | 43.16 | 42.32 | 30.36 | 52.42 |
| LC3B | 42.23 | 41.52 | 28.98 | 46.66 |
| RavZ | 47.60 | 52.33 | 37.52 | 54.44 |
| Water | 43.45 | 43.62 | 38.05 | 52.42 |
| R.m.s deviations | | | | |
| Bond lengths (Å) | 0.007 | 0.009 | 0.007 | 0.003 |
| Bond angles (°) | 1.03 | 1.16 | 0.94 | 0.61 |
| Ramachandran plot | | | | |
| Favored (%) | 96.39 | 98.56 | 99.15 | 90.76 |
| Allowed (%) | 3.61 | 1.44 | 0.85 | 8.43 |
| Outliers (%) | 0 | 0 | 0 | 0.80 |

Values in parentheses are for the highest-resolution shell.

[5] and the LIR2 binding mode in mutNLIR-LC3 (Fig. 2D). Like the p62 LIR motif, negatively charged Asp433 at the $X_{-2}$ position provides additional ionic interactions with Arg11 of LC3B [30]. The binding affinity between CLIR and LC3B is relatively weaker than that between NLIR and LC3B, as shown in our previous paper [22].

### 3.4. A novel conformation of the NLIR motif of RavZ provides an additional ionic interaction with LC3B

The second LIR2 motif possesses Phe29 and Leu32 residues at positions Ω and Ψ, respectively (Fig. 1A). Two residues Asp30 and Leu31 occupy positions $x_1$ and $x_2$, respectively, between the characteristic aromatic and hydrophobic residues. Interestingly, we identified an additional ionic interaction between RavZ and LC3B (Fig. 2B). The side chain oxygen atoms of Asp30 of RavZ interact with the nitrogen atom of His27 of LC3B. Among Atg8 orthologue proteins, LC3A and LC3B possess a histidine residue at position 27, whereas the LC3C isoform possesses a phenylalanine residue at the corresponding position (Fig. 3A). The His27 residue makes bipartite interactions with Asp30 of LIR2 as well as Glu18 of LIR1, indicating that position $x_1$ of LIR2 and $x_2$ of LIR1 are involved in recognition of the particular histidine residue of LC3B. Previous studies reported that negatively charged residues at positions $X_{-1}$ and $X_{-2}$ play a critical role in binding LC3B, however, this is the first report to indicate that a negatively charged residue at a distant location participates in the recognition of LC3B. To confirm this additional ionic interaction, we performed surface plasmon resonance (SPR) experiments with immobilized RavZ using LC3B wild-type (WT) and the H27A mutant (Fig. 3B and C). Surprisingly, the $K_D$ between the H27A mutant and RavZ was 3.2 μM, while that between WT and RavZ was only 307 nM, thus the H27A mutant displayed an approximate 10-fold reduction in affinity relative to WT. Interestingly, the equivalent residue in LC3C possesses no hydrophilic moiety and it displayed much lower affinity relative to LC3B WT (Fig. 3D). Furthermore, consistent with previous report [13], we also found that RavZ binds strongly to GABARAP (Fig. 3E and F), which possesses tyrosine residue at the equivalent position (Fig. 3A). This clearly shows that the unique β-sheet conformation of the LIR motif contributes to stronger affinity *via* additional ionic (or polar) interactions.

## 4. Discussion

The group of Atg8-family member proteins which includes Ubl protein are able to interact with various partners to function in the process of autophagy. This interaction occurs *via* a conserved motif referred to as the LIR motif (or AIM: Atg8-Interacting Motif). There are three LIR motifs in RavZ from *Legionella pneumophila*, and all three motifs have two acidic residues before the $X_{-2}$-$X_{-1}$-(W/F/Y)- $x_1$-$x_2$-(L/I/V)- motif which bind to the basic side chains of LC3B, found in many canonical LC3B and LIR interactions [5,30,31]. Two tandem LIR motifs (LIR1 and LIR2) in NLIR have a shared F-$x_1$-$x_2$-L sequence and, interestingly, acidic residues in between (Fig. 1A). The acidic residues Glu18 ($x_2$) and Asp30 ($x_1$) from each LIR motif were found to participate in additional LC3B interactions in our NLIR-LC3B structure (Fig. 2B). Although the aforementioned acidic

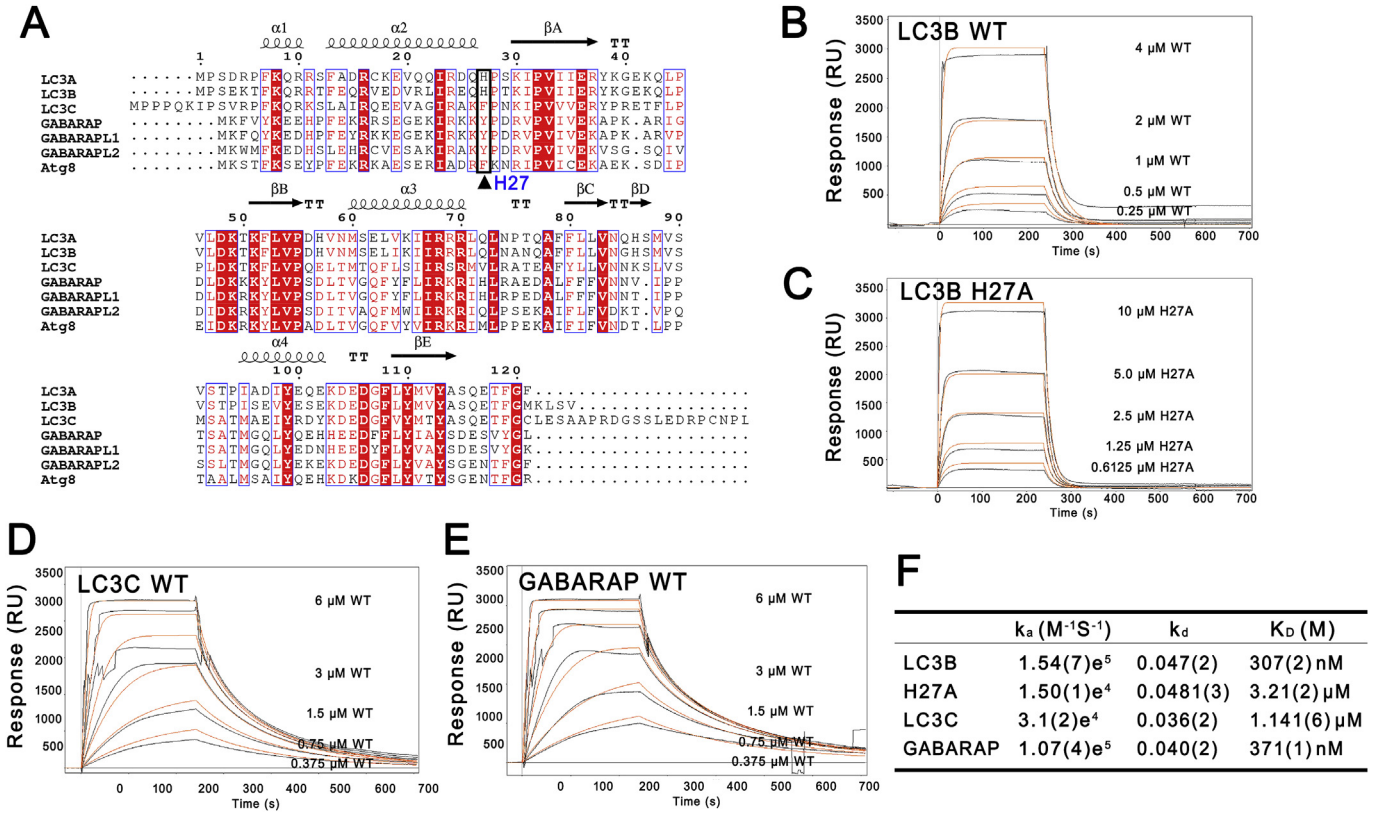


| | $k_a$ ($M^{-1}S^{-1}$) | $k_d$ | $K_D$ (M) |
|---|---|---|---|
| LC3B | 1.54(7)e$^5$ | 0.047(2) | 307(2) nM |
| H27A | 1.50(1)e$^4$ | 0.0481(3) | 3.21(2) μM |
| LC3C | 3.1(2)e$^4$ | 0.036(2) | 1.141(6) μM |
| GABARAP | 1.07(4)e$^5$ | 0.040(2) | 371(1) nM |

**Fig. 3.** Specific ionic interaction mediated by His27 of LC3B. (A) Sequence alignment of Atg8-family members. Three LC3 isoforms LC3A, LC3B and LC3C and three GABARAP members GABARAP, GABARAPL1 and GABARAPL2 (also known as GATE-16) are from humans and Atg8 is from yeast. Boxes indicate residues that are identical (red shading) or highly conserved (red font) in all sequences. Secondary structural elements (α-helices and β-strands) are shown above the sequence alignment and every 10th residue of LC3B is marked with a dot and labeled. The critical His27 residue engaged in interactions with NLIR is indicated by a filled triangle. (B–E) Sensorgram of SPR experiments. The binding affinity of LC3B WT (B), H27A mutant (C), LC3C WT (D), and GABARAP WT (E) with immobilized RavZ was measured. (F) Summary of SPR data. The equilibrium dissociation constant ($K_D$) was obtained by dividing the dissociation rate constant ($k_d$) by the association rate constant ($k_a$). (For interpretation of the references to colour in this figure legend, the reader is referred to the web version of this article.)

residues are located at some distance in the primary sequence, formation of a novel β-sheet conformation within NLIR positions these residues close to the key His27 of LC3B for additional interactions. Thus, NLIR displays higher affinity compared with the canonical LIR and LC3B interaction. As shown in the sequence alignment of Atg8-family members (Fig. 3A), the histidine residue is only conserved in LC3A and LC3B, and not in LC3C. The corresponding residue of LC3C and yeast Atg8 is hydrophobic phenylalanine, which possesses no proton donor to engage in additional polar interactions. Interestingly, the equivalent residue in all GABARAP-family members is tyrosine, and we speculate that the hydroxyl group of tyrosine in GABARAP may form a similar interaction with the carboxyl groups of Glu18 and Asp30 of NLIR.

The structures of most of the LIR motifs show a canonical LIR conformation, which is also shown in our mutLIR-LC3B and CLIR-LC3B complexes (Fig. 2D and F). However, some proteins possess atypical LIR motifs (Fig. 4). For example, the NDP52 autophagy receptor related to *Salmonella* possesses a non-canonical LIR motif [32]. The LIR motif of NDP52 comprises the '-I-L-V-V-' sequence and lacks an aromatic residue (Fig. 4B). Asp132 at the $X_{-1}$ position can enhance the low affinity resulting from the absence of an aromatic ring residue. Another example is GABARAP in complex with a synthetic peptide. The high affinity peptide was generated using a phage display technique [33]. The three-dimensional complex structure suggests that an interaction is possible between an inverse LIR sequence and LC3B *via* a similar manner that utilizes the hydrophobic binding pocket (Fig. 4C). Recently, it was found that the FYCO1 LIR motif has a C-terminal negatively charged residue (Glu1287) which provides additional ionic interactions (Fig. 4D). Clearly, this differs from the additional N-terminal negatively charged residue in typical LIR motifs [34,35]. Unlike these atypical LIR-Atg8 family member protein interactions, RavZ NLIR has a distinctive conformation for high affinity (Fig. 4A) and it might be beneficial for the efficient blocking of host autophagy. The proteolytic activity of RavZ inactivates the functional cycle of LC3 and GABARAP members by covalent modification, and the cleaved LC3 product is unable to be utilized by the host cysteine protease ATG4B. However, to avoid clearance by autophagy, engulfed bacteria must escape from the phagophore membrane. For this purpose, RavZ may evolve to possess stronger binding affinity for LC3 homologs, except LC3C, using the β-sheet conformation of NLIR and synergistic binding avidity using the canonical CLIR motif.

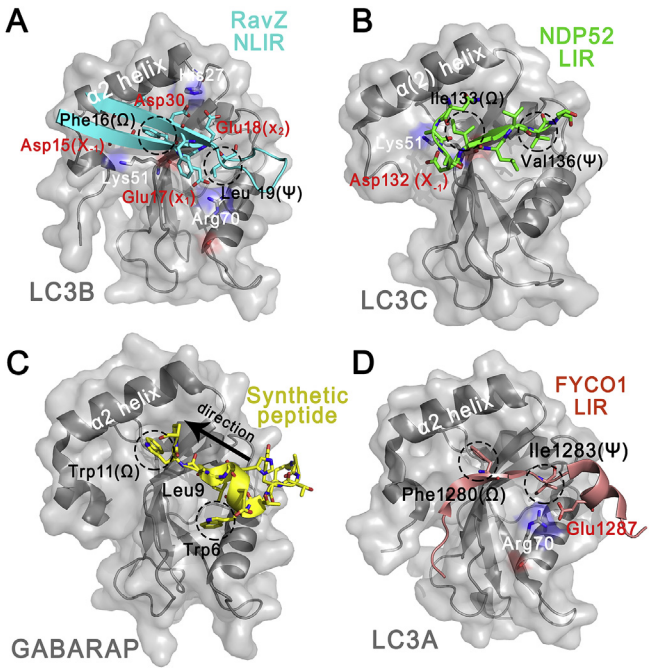


**Fig. 4.** Comparison of atypical LIR conformation bound to Atg8-family member proteins. (A) Structure of our NLIR-LC3B complex. Bound NLIR from RavZ is colored cyan. (B) Structure of LC3C in complex with NDP52 LIR. Bound LIR motif from NDP52 is colored green. Although the LIR motif of NDP52 lacks an aromatic ring residue, Asp132 (position X-$_1$) provides additional affinity with LC3C. (C) Structure of GABARAP in complex with synthetic peptide. Bound synthetic peptide is colored yellow. The orientation of the bound synthetic peptide shows a reverse direction. Trp11 is located on hydrophobic patch 1, however Leu9 is bound on hydrophobic patch 2 with another hydrophobic residue Trp6. (D) Structure of LC3A in complex with the FYCO1 LIR motif. Phe1280 and Ile1283 residues at positions Ω and Ψ bind to hydrophobic patches 1 and 2, respectively. Additionally, negatively charged Glu1287 following the LIR motif interacts with positively charged Arg70 of LC3A. All Atg8-family member proteins are presented as gray transparent surfaces and the critical α2 helices are indicated. Residues belonging to the Atg8-family are labeled white, while residues at positions Ω and Ψ of the LIR motif are labeled black with a dashed circle. The negatively charged residues in the LIR motif utilized for additional interactions are labeled and colored red. (For interpretation of the references to colour in this figure legend, the reader is referred to the web version of this article.)

## Acknowledgements

We thank the staff at beamline 5C, Pohang Accelerator Laboratory, Korea and at beamline NE3A, Photon Factory, Japan for help with the X-ray data collection. This work was supported by National Research Foundation of Korea grants (NRF-2016R1E1A1A01942623 and BRL grant: No. 2015041919). This research was also supported by a Korea University Future Research Grant (K1614811).

## Transparency document

Transparency document related to this article can be found online at http://dx.doi.org/10.1016/j.bbrc.2017.06.173.

## Appendix A. Supplementary data

Supplementary data related to this article can be found at http://dx.doi.org/10.1016/j.bbrc.2017.06.173.

## Accession numbers

Atomic coordinates and structure factor files have been deposited in the Protein Data Bank under the following accession codes: 5XAD, 5XAE and 5XAC for NLIR-LC3, mutNLIR-LC3B and CLIR-LC3B, respectively.

## References

[1] D.J. Klionsky, S.D. Emr, Cell biology - autophagy as a regulated pathway of cellular degradation, Science 290 (2000) 1717–1721.
[2] H. Nakatogawa, K. Suzuki, Y. Kamada, Y. Ohsumi, Dynamics and diversity in autophagy mechanisms: lessons from yeast, Nat. Rev. Mol. Cell Biol. 10 (2009) 458–467.
[3] T. Johansen, T. Lamark, Selective autophagy goes exclusive, Nat. Cell Biol. 16 (2014) 395–397.
[4] G. Zaffagnini, S. Martens, Mechanisms of selective autophagy, J. Mol. Biol. 428 (2016) 1714–1724.
[5] B.W. Kim, H. Kwon do, H.K. Song, Structure biology of selective autophagy receptors, BMB Rep. 49 (2016) 73–80.
[6] S. Svenning, T. Johansen, Selective autophagy, Essays Biochem. 55 (2013) 79–92.
[7] A. Khaminets, C. Behl, I. Dikic, Ubiquitin-dependent and independent signals in selective autophagy, Trends Cell Biol. 26 (2016) 6–16.
[8] K.A. Bauckman, N. Owusu-Boaitey, I.U. Mysorekar, Selective autophagy: xenophagy, Methods 75 (2015) 120–127.
[9] K. Mao, D.J. Klionsky, Xenophagy: a battlefield between host and microbe, and a possible avenue for cancer treatment, Autophagy 13 (2017) 223–224.
[10] B.W. Kim, S.B. Hong, J.H. Kim, H. Kwon do, H.K. Song, Structural basis for recognition of autophagic receptor NDP52 by the sugar receptor galectin-8, Nat. Commun. 4 (2013) 1613.
[11] P. Chandra, D. Kumar, Selective autophagy gets more selective: uncoupling of autophagy flux and xenophagy flux in Mycobacterium tuberculosis-infected macrophages, Autophagy 12 (2016) 608–609.
[12] N. von Muhlinen, T. Thurston, G. Ryzhakov, S. Bloor, F. Randow, NDP52, a novel autophagy receptor for ubiquitin-decorated cytosolic bacteria, Autophagy 6 (2010) 288–289.
[13] A. Choy, J. Dancourt, B. Mugo, T.J. O'Connor, R.R. Isberg, T.J. Melia, C.R. Roy, The Legionella effector RavZ inhibits host autophagy through irreversible Atg8 deconjugation, Science 338 (2012) 1072–1076.
[14] K. Sugawara, N.N. Suzuki, Y. Fujioka, N. Mizushima, Y. Ohsumi, F. Inagaki, The crystal structure of microtubule-associated protein light chain 3, a mammalian homologue of Saccharomyces cerevisiae Atg8, Genes cells. 9 (2004) 611–618.
[15] Y.J. Jeong, B.C. Jeong, H.K. Song, Crystal structure of ubiquitin-like small archaeal modifier protein 1 (SAMP1) from Haloferax volcanii, Biochem. Biophys. Res. Commun. 405 (2011) 112–117.
[16] S.B. Hong, B.W. Kim, K.E. Lee, S.W. Kim, H. Jeon, J. Kim, H.K. Song, Insights into noncanonical E1 enzyme activation from the structure of autophagic E1 Atg7 with Atg8, Nat. Struct. Mol. Biol. 18 (2011) 1323–1330.
[17] N.N. Noda, K. Satoo, Y. Fujioka, H. Kumeta, K. Ogura, H. Nakatogawa, Y. Ohsumi, F. Inagaki, Structural basis of Atg8 activation by a homodimeric E1, Atg7, Mol. Cell 44 (2011) 462–475.
[18] L. Cappadocia, C.D. Lima, Ubiquitin-like protein conjugation: structures, chemistry, and mechanism, Chem. Rev. (2017), http://dx.doi.org/10.1021/acs.chemrev.6b00737.
[19] N.N. Noda, F. Inagaki, Mechanisms of autophagy, Annu. Rev. Biophys. 44 (2015) 101–122.
[20] A. Choy, C.R. Roy, Autophagy and bacterial infection: an evolving arms race, Trends Microbiol. 21 (2013) 451–456.
[21] F.A. Horenkamp, K.J. Kauffman, L.J. Kohler, R.K. Sherwood, K.P. Krueger, V. Shteyn, C.R. Roy, T.J. Melia, K.M. Reinisch, The Legionella anti-autophagy effector RavZ targets the autophagosome via PI3P- and curvature-sensing motifs, Dev. Cell 34 (2015) 569–576.
[22] D.H. Kwon, S. Kim, Y.O. Jung, et al., The 1:2 complex between RavZ and LC3 reveals a mechanism for deconjugation of LC3 on the phagophore membrane, Autophagy 13 (2017) 70–81.
[23] A. Yang, S. Pantoom, Y.W. Wu, Elucidation of the anti-autophagy mechanism of the Legionella effector RavZ using semisynthetic LC3 proteins, Elife 6 (2017).
[24] S. Pantoom, A. Yang, Y.W. Wu, Lift and cut: anti-host autophagy mechanism of Legionella pneumophila, Autophagy (2017) 0.
[25] N.N. Noda, Y. Ohsumi, F. Inagaki, Atg8-family interacting motif crucial for selective autophagy, Febs Lett. 584 (2010) 1379–1385.
[26] A.B. Birgisdottir, T. Lamark, T. Johansen, The LIR motif - crucial for selective autophagy, J. Cell Sci. 126 (2013) 3237–3247.
[27] V.V. Rogov, H. Suzuki, E. Fiskin, et al., Structural basis for phosphorylation-triggered autophagic clearance of Salmonella, Biochem. J. 454 (2013) 459–466.
[28] H. Suzuki, K. Tabata, E. Morita, M. Kawasaki, R. Kato, R.C. Dobson, T. Yoshimori, S. Wakatsuki, Structural basis of the autophagy-related LC3/Atg13 LIR complex: recognition and interaction mechanism, Structure 22 (2014) 47–58.
[29] F. Wu, P. Wang, Y. Shen, N.N. Noda, H. Zhang, Small differences make a big impact: structural insights into the differential function of the 2 Atg8 homologs in C. elegans, Autophagy 12 (2016) 606–607.
[30] Y. Ichimura, T. Kumanomidou, Y.S. Sou, et al., Structural basis for sorting

mechanism of p62 in selective autophagy, J. Biol. Chem. 283 (2008) 22847–22857.
[31] S. Pankiv, T.H. Clausen, T. Lamark, A. Brech, J.A. Bruun, H. Outzen, A. Overvatn, G. Bjorkoy, T. Johansen, p62/SQSTM1 binds directly to Atg8/LC3 to facilitate degradation of ubiquitinated protein aggregates by autophagy, J. Biol. Chem. 282 (2007) 24131–24145.
[32] N. von Muhlinen, M. Akutsu, B.J. Ravenhill, A. Foeglein, S. Bloor, T.J. Rutherford, S.M. Freund, D. Komander, F. Randow, LC3C, bound selectively by a noncanonical LIR motif in NDP52, is required for antibacterial autophagy, Mol. Cell 48 (2012) 329–342.
[33] O.H. Weiergraber, T. Stangler, Y. Thielmann, J. Mohrluder, K. Wiesehan, D. Willbold, Ligand binding mode of GABAA receptor-associated protein, J. Mol. Biol. 381 (2008) 1320–1331.
[34] X. Cheng, Y. Wang, Y. Gong, F. Li, Y. Guo, S. Hu, J. Liu, L. Pan, Structural basis of FYCO1 and MAP1LC3A interaction reveals a novel binding mode for Atg8-family proteins, Autophagy 12 (2016) 1330–1339.
[35] S. Sakurai, T. Tomita, T. Shimizu, U. Ohto, The crystal structure of mouse LC3B in complex with the FYCO1 LIR reveals the importance of the flanking region of the LIR motif, Acta Crystallogr. F. Struct. Biol. Commun. 73 (2017) 130–137.